Supplementary Information

Hydropyrolysis: towards fluorescence-free Raman spectroscopy analysis of internal diesel injector deposits

Joel Viggars,[a] Sarah Angel-Smith,[a] Graham A. Rance,[b,c] Ahmed Khairy,[a,d] Will Meredith,[a] Adrienne Davies,[b] Jim Barker,[e*] Jaqueline Reid,[e] David J. Scurr[f] and Colin E. Snape[a]

a. Faculty of Engineering, University of Nottingham, Energy Technologies Building, Innovation Park, Jubilee Campus, Triumph Road, Nottingham NG7 2TU, UK

b. School of Chemistry, University of Nottingham, University Park, Nottingham, NG7 2RD, UK

c. Nanoscale and Microscale Research Centre (nmRC), University of Nottingham, University Park, Nottingham, NG7 2RD, UK

d. Geology Department, Faculty of Science, South Valley University, Qena, 83523, Egypt

e. Innospec Ltd, Manufacturing Park/Oil Sites Rd, Ellesmere Port, CH65 4EY, UK

f. Laboratory of Pharmacy, University of Nottingham, Nottingham NG7 2RD, UK

* Corresponding author e-mail: jim.barker@innospecinc.com

S1. The effect of laser power on the Raman spectra of the reference carbons

Experiment:

A Raman spectrum at a single fixed location was acquired at P = 0.4, 4.0, 10.0, 20.0 and 40.0 mW for each of the six reference carbons. The acquisition time per spectrum was scaled to laser power, i.e., 60.0, 6.0, 2.4, 1.2 and 0.6 s for P = 0.4, 4.0, 10.0, 20.0 and 40.0 mW, respectively.

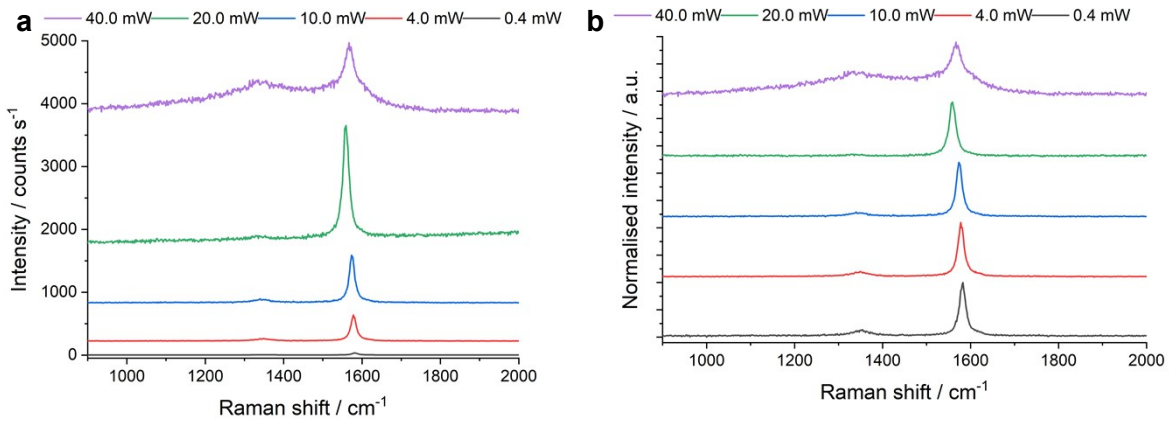

Figure S1. The effect of laser power (P = 0.4–10.0 mW) on the Raman spectrum (λ = 532 nm) of graphite. The spectra presented in (a) have not been processed and in (b) have been processed as described in the Experimental section. Here, I_{base} = 1.6, 12.1, 24.3, 312.0 and 215.9 counts s^{-1} at P = 0.4, 4.0, 10.0, 20.0 and 40.0 mW, respectively.

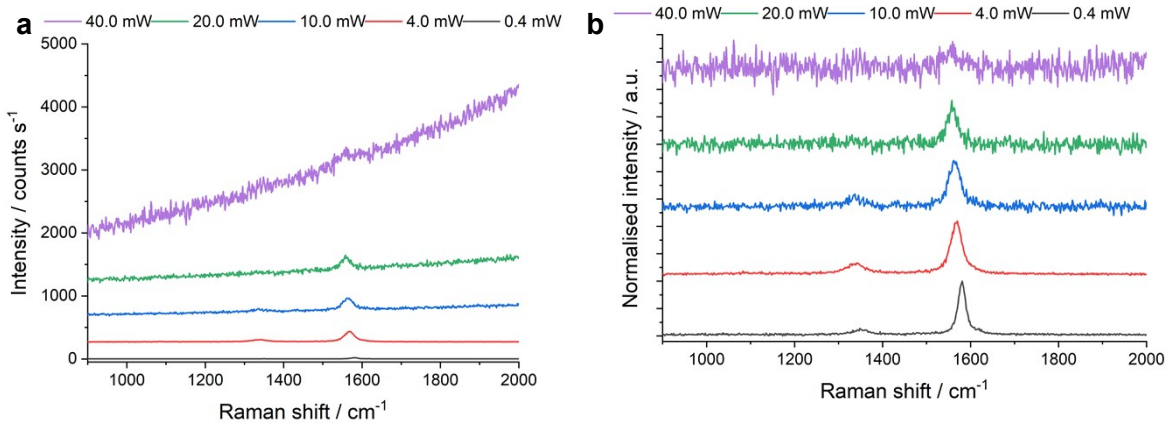

Figure S2. The effect of laser power (P = 0.4–10.0 mW) on the Raman spectrum (λ = 532 nm) of MWCNT. The spectra presented in (a) have not been processed and in (b) have been processed as

described in the Experimental section. Here, I_{base} = 1.5, 15.3, 265.1, 591.1 and 3977.6 counts s^{-1} at P = 0.4, 4.0, 10.0, 20.0 and 40.0 mW, respectively.

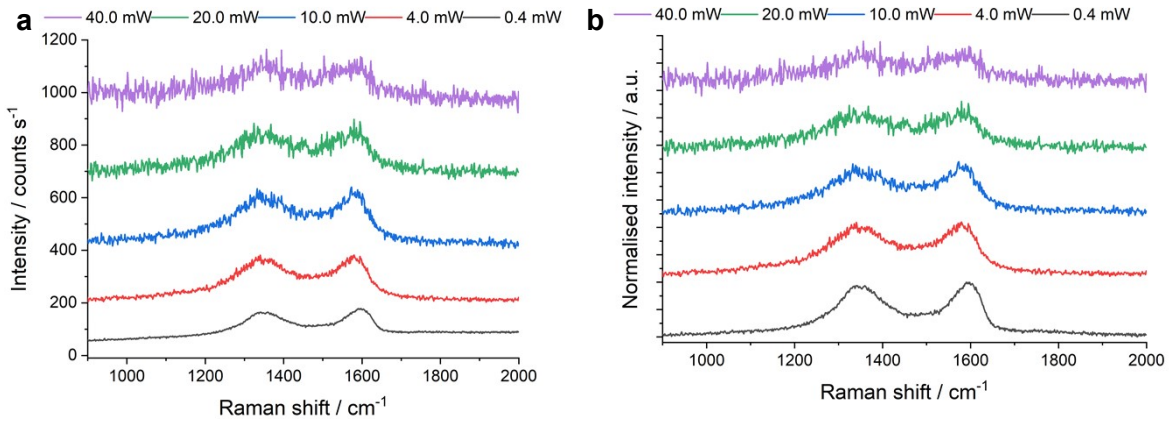

Figure S3. The effect of laser power (P = 0.4–10.0 mW) on the Raman spectrum (λ = 532 nm) of GO. The sample was photobleached for 100 s at p = 0.4 mW prior to spectrum acquisition to suppress some of the observed fluorescence. The spectra presented in (a) have not been processed and in (b) have been processed as described in the Experimental section. Here, I_{base} = 85.0, 66.5, 109.1, 157.6 and 151.2 counts s^{-1} at P = 0.4, 4.0, 10.0, 20.0 and 40.0 mW, respectively.

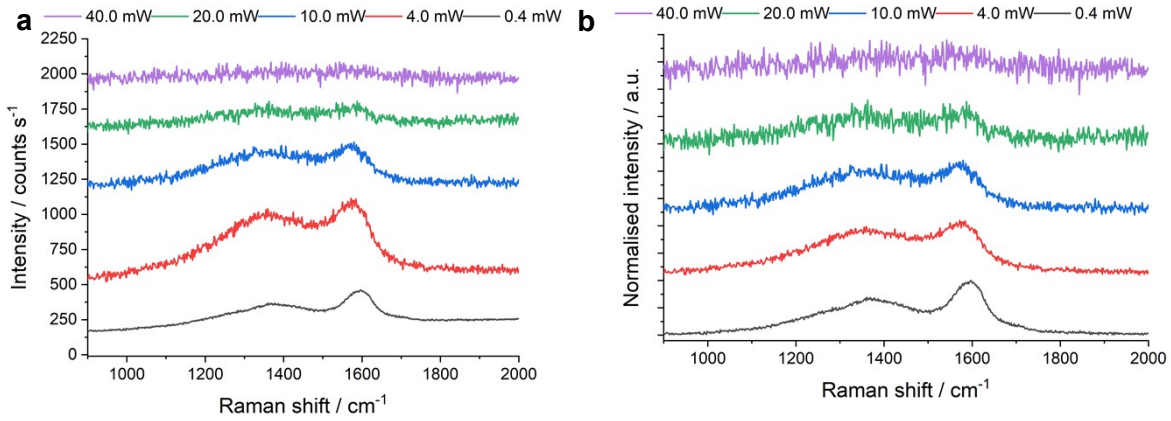

Figure S4. The effect of laser power (P = 0.4–10.0 mW) on the Raman spectrum (λ = 532 nm) of charcoal. The spectra presented in (a) have not been processed and in (b) have been processed as described in the Experimental section. Here, I_{base} = 252.8, 579.6, 330.4, 291.5 and 211.6 s^{-1} at P = 0.4, 4.0, 10.0, 20.0 and 40.0 mW, respectively.

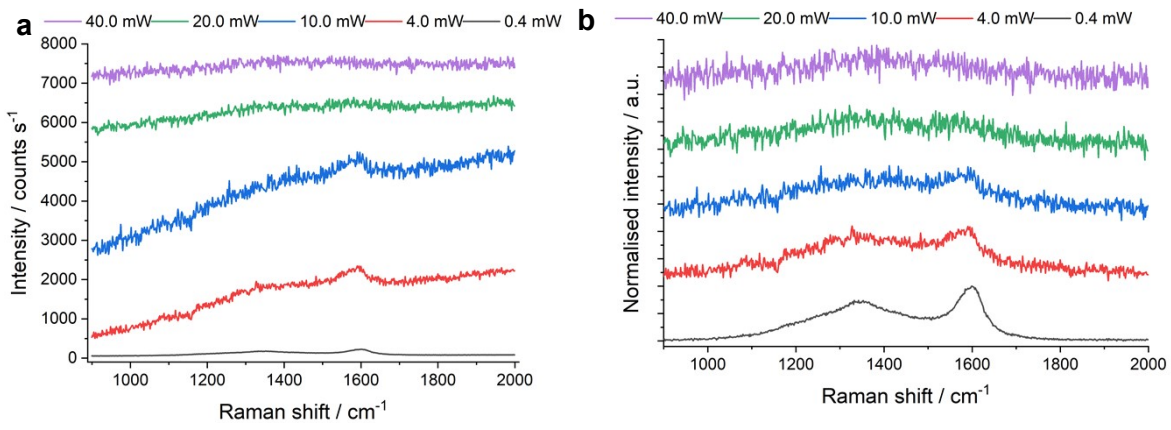

Figure S5. The effect of laser power (P = 0.4–10.0 mW) on the Raman spectrum (λ = 532 nm) of Biochar-A. The spectra presented in (a) have not been processed and in (b) have been processed as described in the Experimental section. Here, I_{base} = 82.1, 7813.1, 12477.0, 3681.8 and 2276.0 counts s^{-1} at P = 0.4, 4.0, 10.0, 20.0 and 40.0 mW, respectively.

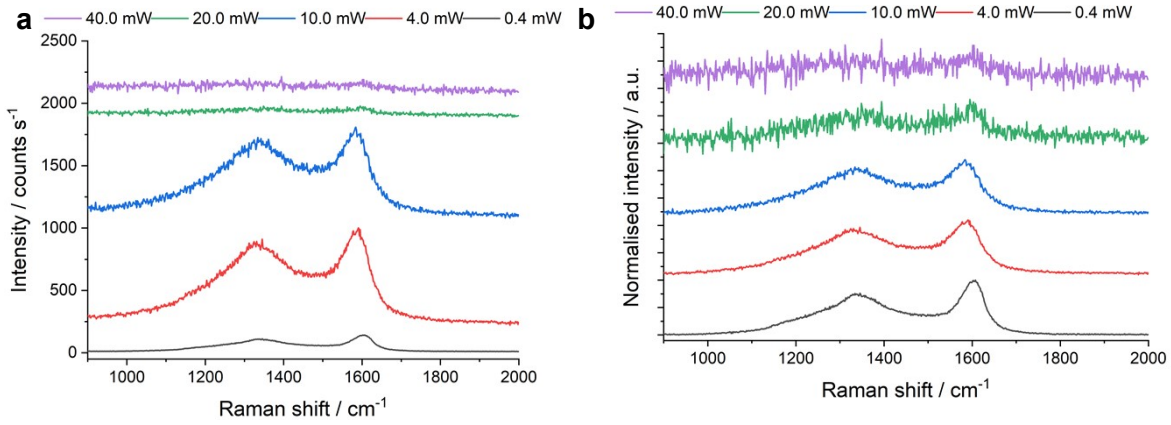

Figure S6. The effect of laser power (P = 0.4–10.0 mW) on the Raman spectrum (λ = 532 nm) of Biochar-B. The spectra presented in (a) have not been processed and in (b) have been processed as described in the Experimental section. Here, I_{base} = 10.9, 152.0, 160.9, 49.7 and 103.7 counts s^{-1} at P = 0.4, 4.0, 10.0, 20.0 and 40.0 mW, respectively.

Conclusions:

In general, where the laser power exceeds 0.4 mW, the following spectral changes are observed: (i) a shift in the position of the G band to lower Raman shift, consistent with laser-induced heating; (ii) a change in I_D:I_G, reflecting structural ordering of the carbon in response to laser heating; and (iii) a variable change in baseline intensity.

At higher laser powers, more dramatic spectral changes are seen, including broadening of all bands, increases in the baseline intensity, and, in the extreme cases, near total loss of signal,

indicative of further photothermal transformation and ultimately combustion of the carbons.

Comparing the six samples, it appears that more ordered carbons (e.g., graphite and MWCNT) have a higher threshold for laser-promoted heating and subsequent photothermally-induced restructuring than more disordered carbons (e.g., GO, charcoal and the two Biochars).

S2. The effect of laser wavelength on the Raman spectra of the reference carbons

Experiment:

A Raman spectrum (P ≤ 0.4 mW) was acquired at λ = 325, 532, 660 and 785 nm from 3-5 random locations for each of the six reference carbons.

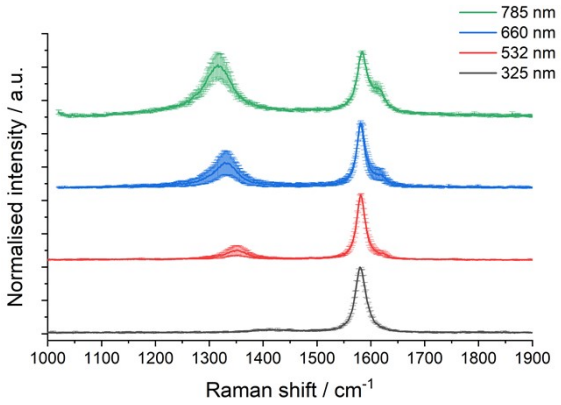

Figure S7. The effect of laser wavelength (λ = 325, 532, 660 and 785 nm) on the Raman spectra (P ≤ 0.4 mW) of graphite. The spectra presented are the mean with error bars reflecting one standard deviation from N=5 measurements for λ = 532 nm and N = 3 measurements for λ = 325, 660 and 785 nm. Each spectrum was processed according to the description in the Experimental section.

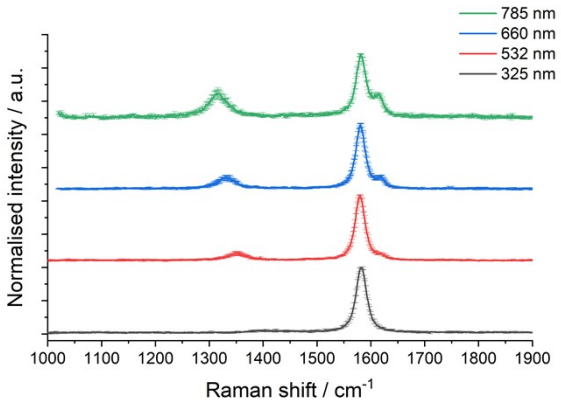

Figure S8. The effect of laser wavelength (λ = 325, 532, 660 and 785 nm) on the Raman spectra (P ≤ 0.4 mW) of MWCNT. The spectra presented are the mean with error bars reflecting one standard deviation from N=5 measurements for λ = 532 nm and N = 3 measurements for λ = 325, 660 and 785 nm. Each spectrum was processed according to the description in the Experimental section.

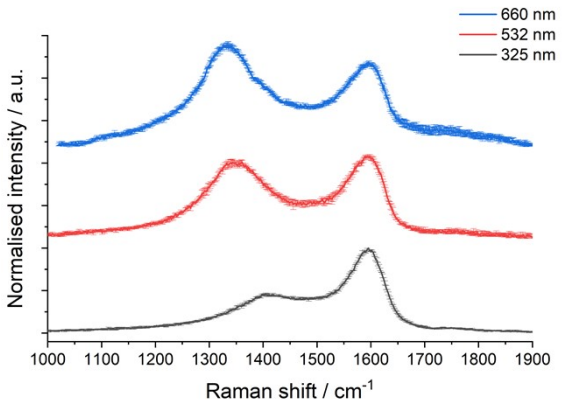

Figure S9. The effect of laser wavelength (λ = 325, 532 and 660 nm) on the Raman spectra (P ≤ 0.4 mW) of GO. For spectra obtained at λ = 532 and 660 nm, the sample was photobleached for 100 s at P = 0.4 and 0.25 mW, respectively, prior to acquisition to suppress some of the observed fluorescence. It was not possible to record Raman spectra at λ = 785 nm due to dominant fluorescence. The spectra presented are the mean with error bars reflecting one standard deviation from N=5 measurements for λ = 532 nm and N = 3 measurements for λ = 325 and 660 nm. Each spectrum was processed according to the description in the Experimental section.

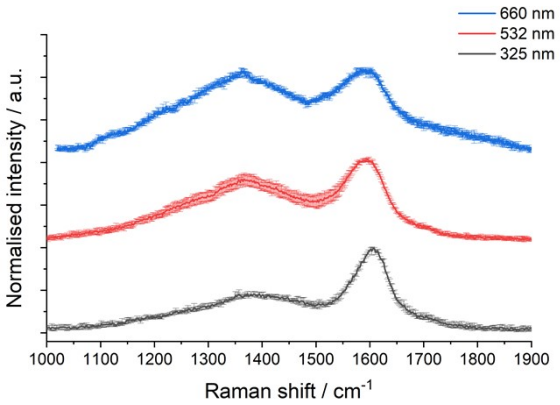

Figure S10. The effect of laser wavelength (λ = 325, 532, and 660 nm) on the Raman spectra (P ≤ 0.4 mW) of charcoal. For spectra obtained at λ = 660 nm, the sample was photobleached for 100 s at P = 0.25 mW prior to acquisition to suppress some of the observed fluorescence. It was not possible to record Raman spectra at λ = 785 nm due to dominant fluorescence. The spectra presented are the mean with error bars reflecting one standard deviation from N=5 measurements for λ = 532 nm and N = 3 measurements for λ = 325 and 660 nm. Each spectrum was processed according to the description in the Experimental section.

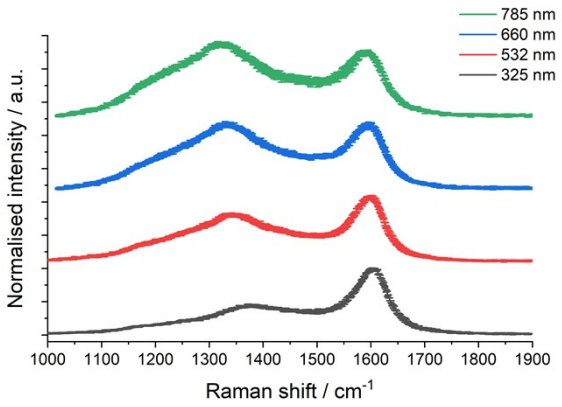

Figure S11. The effect of laser wavelength (λ = 325, 532, 660 and 785 nm) on the Raman spectra (P ≤ 0.4 mW) of Biochar-A. The spectra presented are the mean with error bars reflecting one standard deviation from N=5 measurements for λ = 532 nm and N = 3 measurements for λ = 325, 660 and 785 nm. Each spectrum was processed according to the description in the Experimental section.

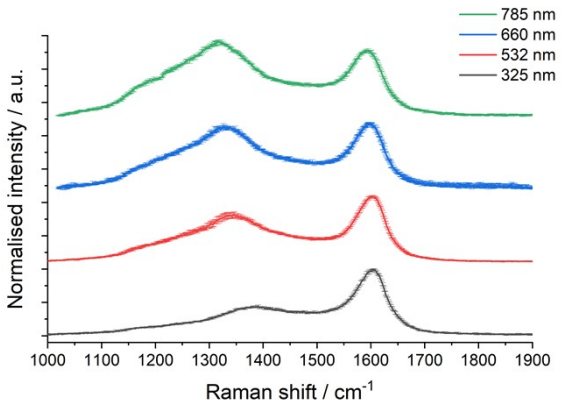

Figure S12. The effect of laser wavelength (λ = 325, 532, 660 and 785 nm) on the Raman spectra (P ≤ 0.4 mW) of Biochar-B. The spectra presented are the mean with error bars reflecting one standard deviation from N=5 measurements for λ = 532 nm and N = 3 measurements for λ = 325, 660 and 785 nm. Each spectrum was processed according to the description in the Experimental section.

Table S1. Spectral characteristics extracted using the peak limits method from the point spectra (λ = 325, 532, 660 and 785 nm) of the reference carbons investigated in this study by μRS before treatment. Values are quoted as mean plus/minus one standard deviation from N=5 measurements for λ = 532 nm and N = 3 measurements for λ = 325, 660 and 785 nm.

Reference carbon	**λ / nm**	**I_{base} / counts s^{-1}**	**D band**		**G band**		**I_D:I_G**
			Position / cm^{-1}	**Width / cm^{-1}**	**Position / cm^{-1}**	**Width / cm^{-1}**	
Graphite	325	9.7 ± 0.8	1417.0 ± 16.5	107.1 ± 25.7	1579.8 ± 0.0	26.5 ± 0.0	0.07 ± 0.01
	532	1.8 ± 0.1	1351.9 ± 2.6	52.0 ± 3.7	1581.3 ± 1.3	21.4 ± 2.5	0.17 ± 0.07
	660	0.8 ± 0.1	1328.9 ± 1.3	58.4 ± 3.9	1581.3 ± 1.3	23.5 ± 5.5	0.41 ± 0.19
	785	1.3 ± 0.2	1316.9 ± 2.3	71.2 ± 8.5	1584.2 ± 0.0	37.5 ± 11.6	0.80 ± 20
MWCNT	325	11.0 ± 1.0	1441.3 ± 52.2	55.8 ± 41.9	1583.3 ± 1.3	26.5 ± 2.2	0.06 ± 0.01
	532	1.6 ± 0.1	1350.3 ± 2.6	45.6 ± 7.3	1579.4 ± 1.5	23.3 ± 1.5	0.14 ± 0.03
	660	0.7 ± 0.1	1329.4 ± 3.4	49.4 ± 2.2	1580.3 ± 1.3	25.0 ± 1.3	0.19 ± 0.04
	785	0.9 ± 0.0	1314.5 ± 3.9	46.0 ± 3.4	1582.5 ± 1.3	27.2 ± 1.3	0.42 ± 0.07
GO	325	9.6 ± 0.1	1400.7 ± 3.4	169.7 ± 4.5	1595.3 ± 0.0	94.9 ± 3.8	0.46 ± 0.01
	532	92.6 ± 49.3 [a]	1348.0 ± 10.0	163.0 ± 14.2	1593.1 ± 3.2	103.5 ± 6.5	0.93 ± 0.03
	660	219.3 ± 119.1 [a]	1332.7 ± 3.9	155.6 ± 4.7	1596.0 ± 1.3	125.1 ± 2.6	1.22 ± 0.04
	785	- [b]	- [b]	- [b]	- [b]	- [b]	- [b]
Charcoal	325	22.3 ± 3.8	1377.3 ± 19.1	249.4 ± 17.3	1605.3 ± 3.4	89.6 ± 4.6	0.48 ± 0.03
	532	311.8 ± 106.5	1367.8 ± 6.5	269.1 ± 11.7	1598.0 ± 3.6	123.1 ± 15.1	0.77 ± 0.07
	660	501.5 ± 135.3 [a]	1363.1 ± 1.3	281.8 ± 12.5	1586.9 ± 4.6	156.0 ± 3.4	0.98 ± 0.06
	785	- [b]	- [b]	- [b]	- [b]	- [b]	- [b]
Biochar-A	325	9.2 ± 0.3	1377.5 ± 5.9	228.3 ± 9.8	1602.6 ± 1.3	87.4 ± 3.4	0.45 ± 0.01
	532	33.0 ± 29.3	1338.8 ± 7.6	274.6 ± 2.7	1599.2 ± 3.5	84.8 ± 4.7	0.73 ± 0.02
	660	5.4 ± 2.2	1337.2 ± 2.2	264.2 ± 7.2	1596.7 ± 2.5	115.5 ± 7.8	1.00 ± 0.02
	785	10.8 ± 5.3	1319.9 ± 5.7	261.5 ± 32.2	1590.1 ± 4.6	130.3 ± 2.2	1.13 ± 0.00
Biochar-B	325	13.8 ± 0.3	1387.7 ± 2.6	213.2 ± 4.7	1603.8 ± 2.2	81.6 ± 2.2	0.45 ± 0.01
	532	17.1 ± 11.3	1339.8 ± 6.8	236.1 ± 16.7	1603.7 ± 2.3	76.1 ± 1.3	0.73 ± 0.04

	660	12.5 ± 1.8	1330.9 ± 3.4	220.3 ± 9.0	1597.2 ± 3.8	86.0 ± 4.4	0.96 ± 0.01
	785	22.4 ± 3.6	1316.7 ± 0.0	218.3 ± 13.5	1592.8 ± 2.2	98.6 ± 3.4	1.13 ± 0.02

[a] Spectra recorded after 100 s of photobleaching at P ≤ 0.4 mW.

[b] Spectra not recorded.

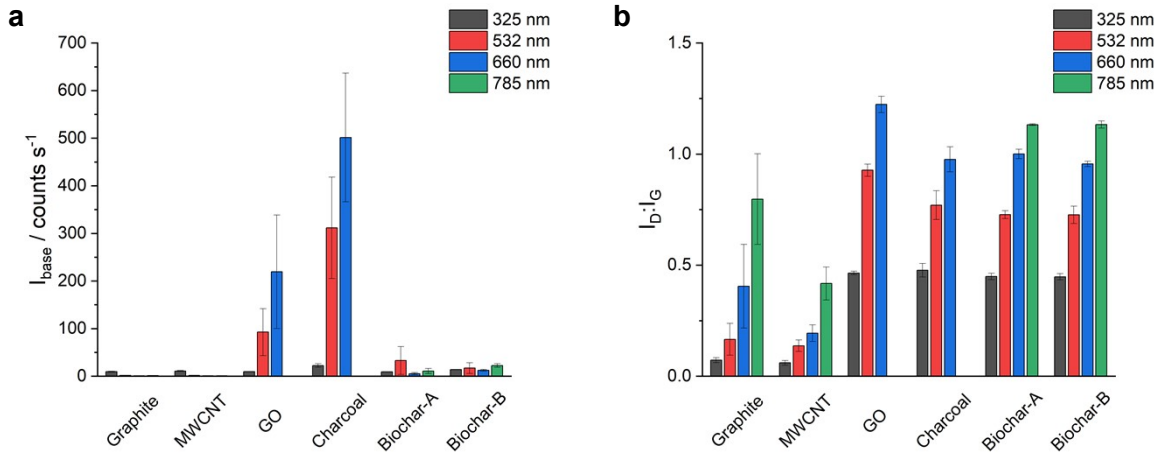

Figure S13. (a) I_{base} and (b) I_D:I_G from λ = 325 (black), 532 (red), 660 (blue) and 785 nm (green) Raman spectra of the reference carbons investigated in this study. Error bars reflect one standard deviation from N=5 measurements for λ = 532 nm and N = 3 measurements for λ = 325, 660 and 785 nm. Prior to spectrum acquisition, GO (λ = 532 and 660 nm) and Charcoal (λ = 660 nm) were photobleached for 100 s at P ≤ 0.4 mW.

Conclusions:

These measurements indicate: (i) the extent of baseline fluorescence, quantified using I_{base}, depends on both the nature of the specific carbon (more ordered carbons, such as graphite and MWCNT, are seemingly less impacted) and the wavelength of the excitation laser (in general, increasing the wavelength increases I_{base}); and (ii) the dispersive nature of the D band and associated sensitivity of both the D band position and I_D:I_G to excitation laser wavelength.

S3. The effect of photobleaching at high laser power on the Raman spectra of the reference carbons

Experiment:

A Raman spectrum (λ = 532 nm) was acquired:

- at P = 0.4 mW (before),
- at P = 0.4 mW, after a 30 s exposure at P = 4.0 mW (after exp 1),
- at P = 0.4 mW, after a further 30 s exposure at P = 10.0 mW (after exp 1+2),
- at P = 0.4 mW, after a further 30 s exposure at P = 20.0 mW (after exp 1+2+3).

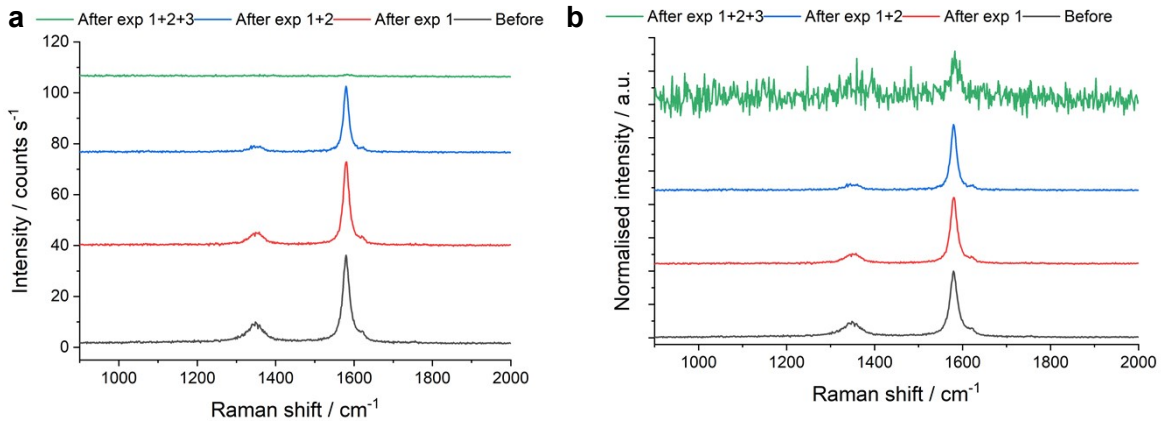

Figure S14. The effect of photobleaching graphite at high laser power. The spectra presented in (a) have not been processed and those presented in (b) have been processed as described in the Experimental section. Here, I_{base} = 1.7, 1.6, 1.5 and 0.8 counts s^{-1} as the experiments progress.

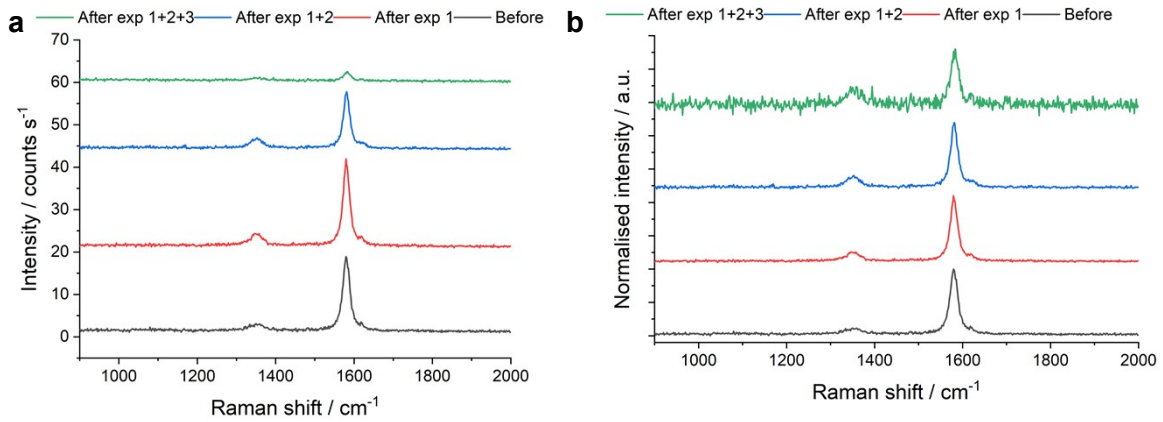

Figure S15. The effect of photobleaching MWCNT at high laser power. The spectra presented in (a) have not been processed and those presented in (b) have been processed as described in the Experimental section. Here, I_{base} = 1.2, 1.3, 1.1 and 0.7 counts s^{-1} as the experiments progress.

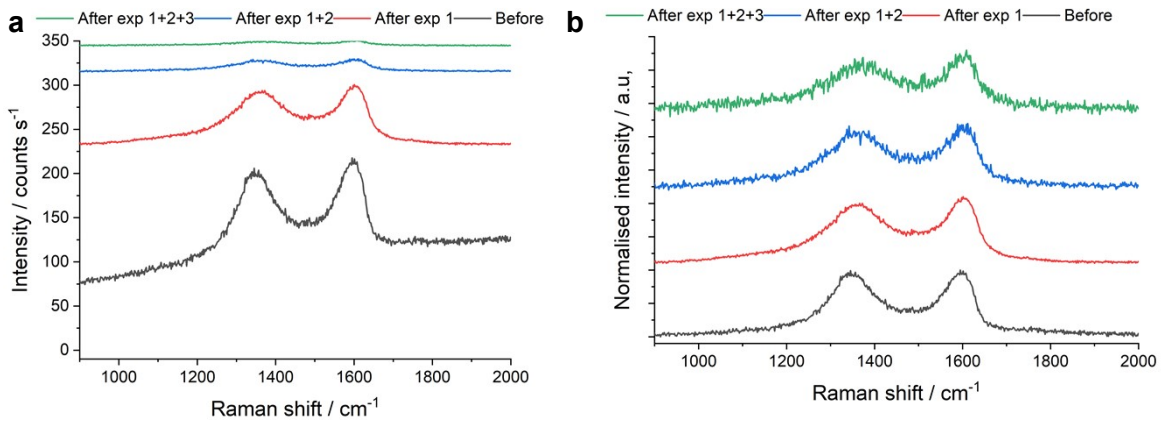

Figure S16. The effect of photobleaching GO at high laser power. The sample was photobleached for 100 s at p = 0.4 mW prior to spectrum acquisition to suppress some of the observed fluorescence. The spectra presented in (a) have not been processed and those presented in (b) have been processed as described in the Experimental section. Here, I_{base} = 124.8, 10.0, 4.7 and 2.6 counts s^{-1} as the experiments progress.

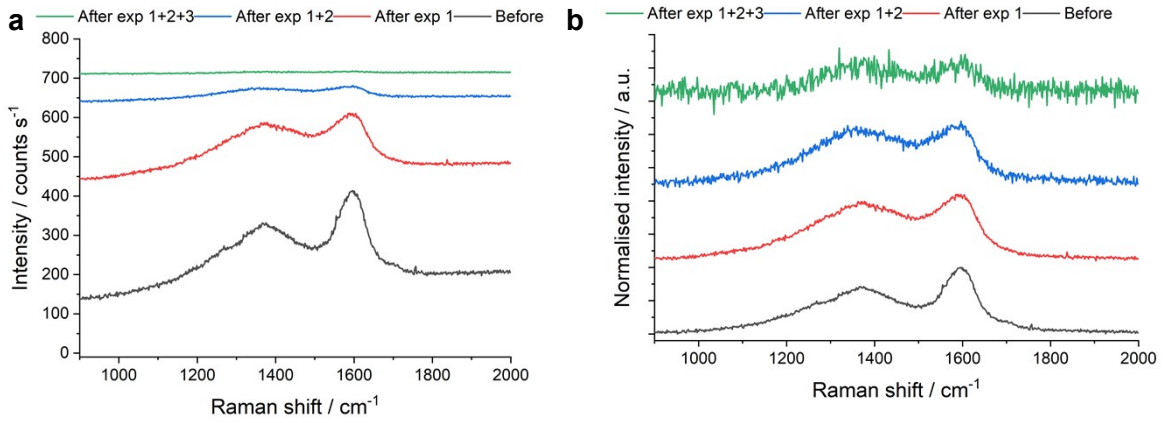

Figure S17. The effect of photobleaching charcoal at high laser power. The spectra presented in (a) have not been processed and those presented in (b) have been processed as described in the Experimental section. Here, I_{base} = 207.7, 124.4, 42.8 and 13.8 counts s^{-1} as the experiments progress.

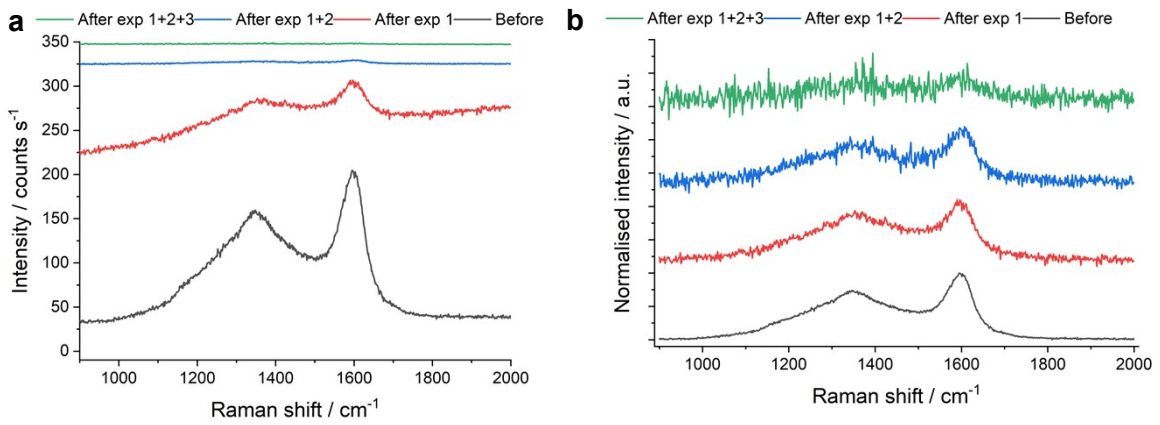

Figure S18. The effect of photobleaching Biochar-A at high laser power. The spectra presented in (a) have not been processed and those presented in (b) have been processed as described in the Experimental section. Here, I_{base} = 38.4, 131.6, 3.3 and 1.7 counts s^{-1} as the experiments progress.

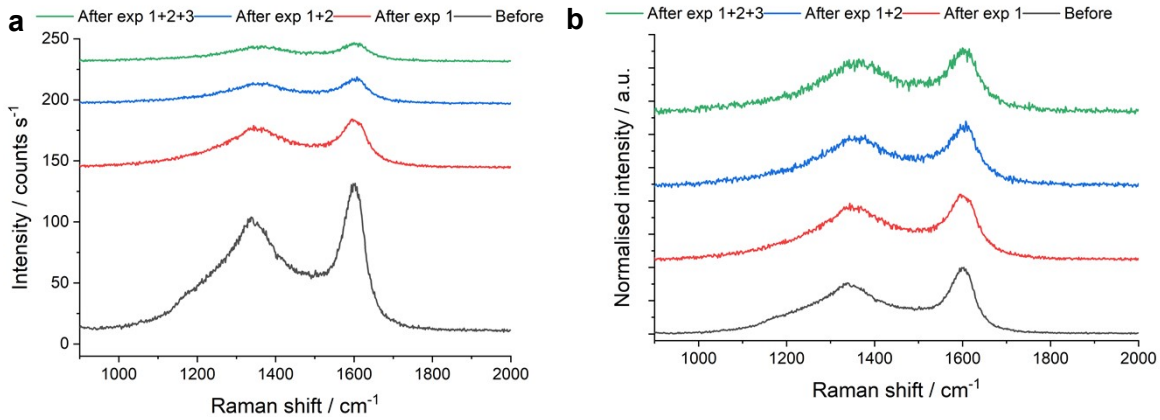

Figure S19. The effect of photobleaching Biochar-B at high laser power. The spectra presented in (a) have not been processed and those presented in (b) have been processed as described in the Experimental section. Here, I_{base} = 12.1, 6.1, 3.8 and 3.2 counts s^{-1} as the experiments progress.

Conclusions:

These experiments indicate that photobleaching carbons at high laser power (P > 0.4 mW) is an ineffective route for fluorescence suppression, as, despite higher powers typically reducing I_{base}, this process results in a variety of irreversible material- and power-dependent changes in the structural organisation of the underlying carbon, and under extreme conditions, photothermally-induced local combustion and sample loss.

S4. The effect of photobleaching at low laser power on the Raman spectra of the reference carbons

Experiment:

A Raman spectrum (acquisition time = 2 s) was obtained every 2.5 s over a 300 s duration and I_{base} (the intensity at 1900 cm^{-1}) extracted at each time point. The experiments were performed separately at λ = 325 (black), 532 (red), 660 (blue) and 785 nm (green).

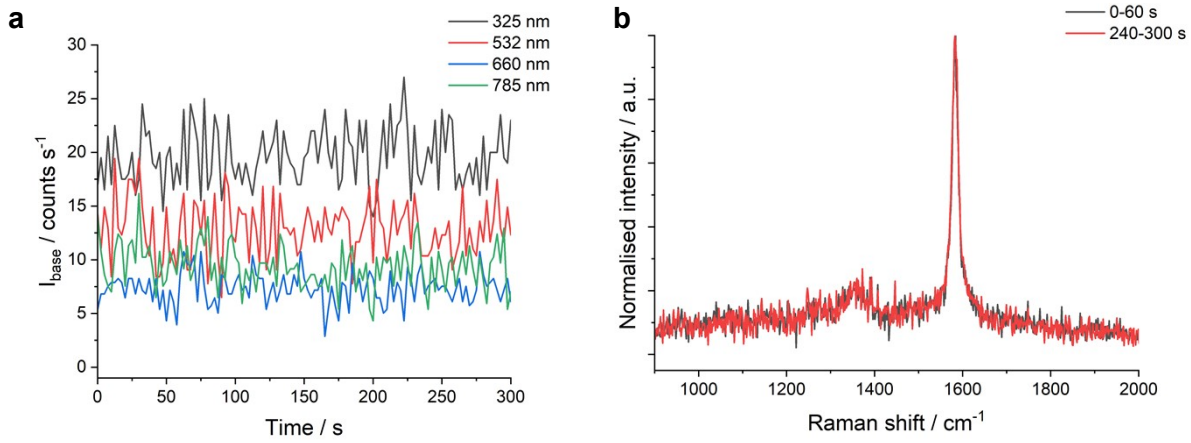

Figure S20. The effect of photobleaching graphite at low power over time. (a) Graphical correlation of I_{base} with time for each of the excitation laser wavelengths explored. (b) The mean Raman spectra (λ = 532 nm) obtained by averaging the spectra collected within the first 60 s (black) and last 60 s (red) of the experiment. The spectra presented in (b) have been processed as described in the Experimental section.

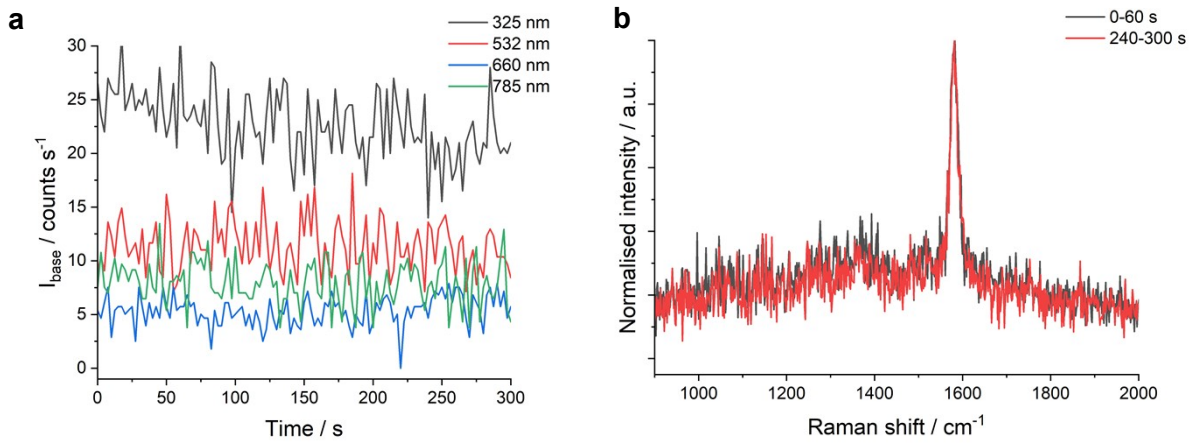

Figure S21. The effect of photobleaching MWCNT at low power over time. (a) Graphical correlation of I_{base} with time for each of the excitation laser wavelengths explored. (b) The mean Raman spectra

(λ = 532 nm) obtained by averaging the spectra collected within the first 60 s (black) and last 60 s (red) of the experiment. The spectra presented in (b) have been processed as described in the Experimental section.

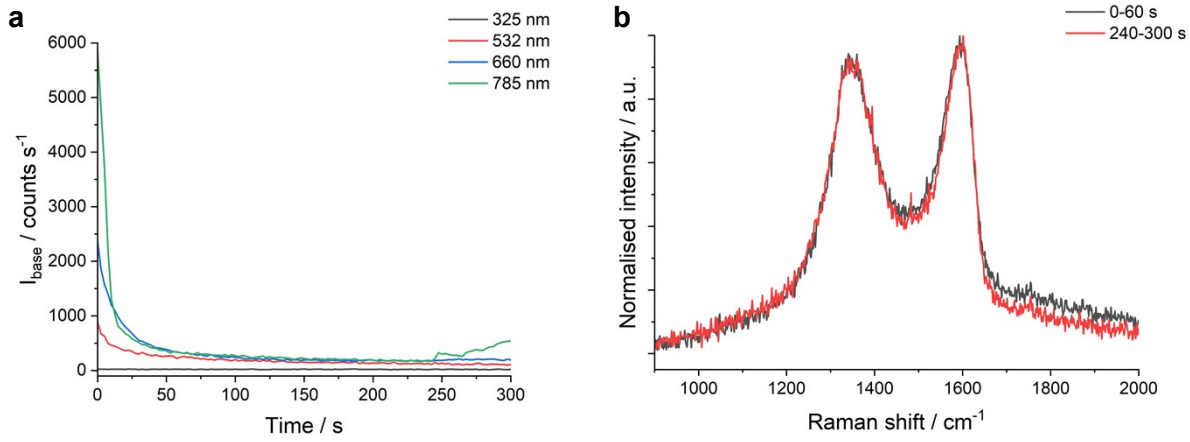

Figure S22. The effect of photobleaching GO at low power over time. (a) Graphical correlation of I_{base} with time for each of the excitation laser wavelengths explored. (b) The mean Raman spectra (λ = 532 nm) obtained by averaging the spectra collected within the first 60 s (black) and last 60 s (red) of the experiment. The spectra presented in (b) have been processed as described in the Experimental section.

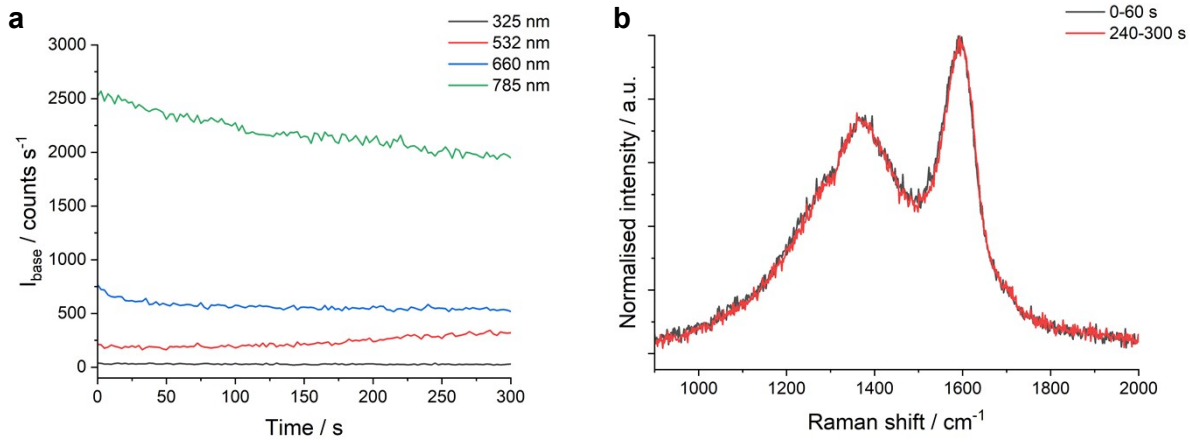

Figure S23. The effect of photobleaching charcoal at low power over time. (a) Graphical correlation of I_{base} with time for each of the excitation laser wavelengths explored. (b) The mean Raman spectra (λ = 532 nm) obtained by averaging the spectra collected within the first 60 s (black) and last 60 s (red) of the experiment. The spectra presented in (b) have been processed as described in the Experimental section.

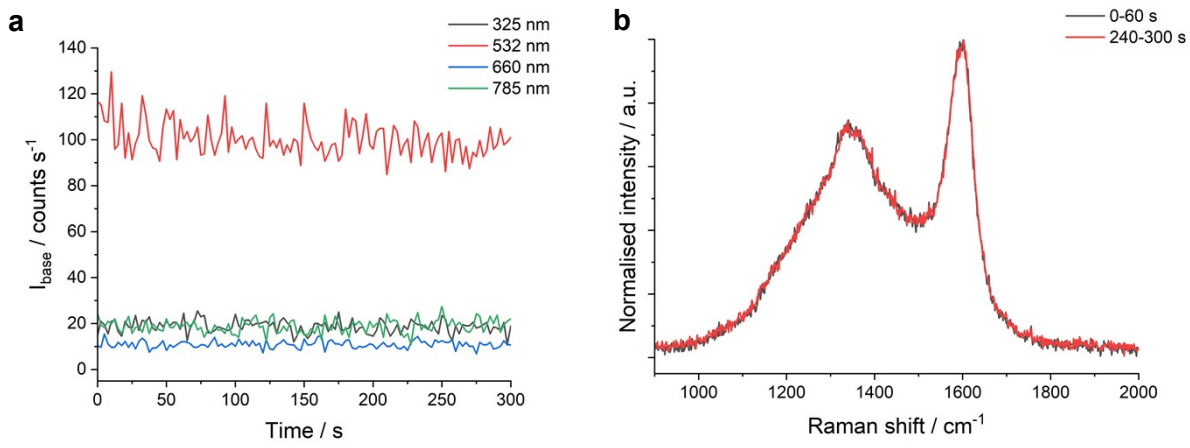

Figure S24. The effect of photobleaching Biochar-A at low power over time. (a) Graphical correlation of I_{base} with time for each of the excitation laser wavelengths explored. (b) The mean Raman spectra (λ = 532 nm) obtained by averaging the spectra collected within the first 60 s (black) and last 60 s (red) of the experiment. The spectra presented in (b) have been processed as described in the Experimental section.

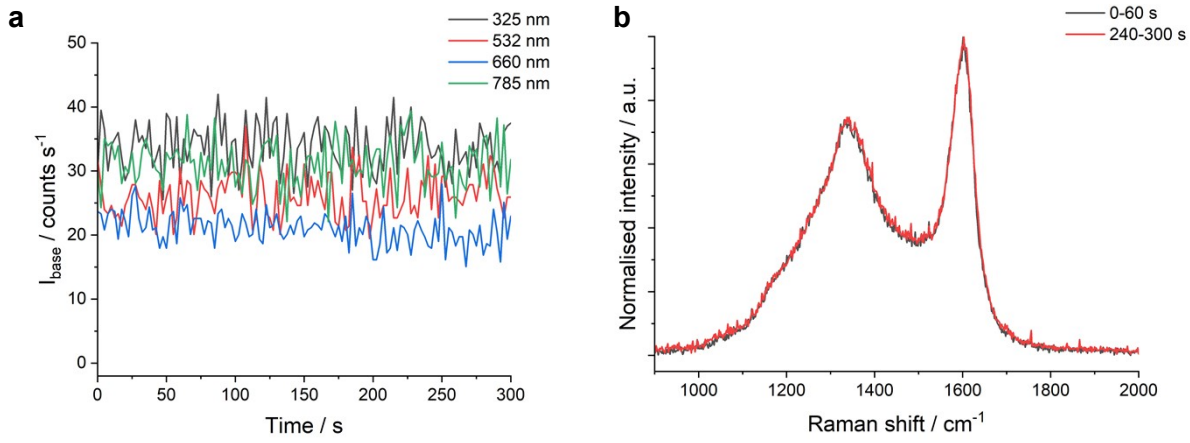

Figure S25. The effect of photobleaching Biochar-B at low power over time. (a) Graphical correlation of I_{base} with time for each of the excitation laser wavelengths explored. (b) The mean Raman spectra (λ = 532 nm) obtained by averaging the spectra collected within the first 60 s (black) and last 60 s (red) of the experiment. The spectra presented in (b) have been processed as described in the Experimental section.

Conclusion:

These experiments indicate that photobleaching at low laser power (P ≤ 0.4 mW): (i) results in no significant changes in the structure of the carbons (in all cases, the spectra obtained at 0-60 s and 240-300 s are effectively identical); and (ii) represents a tool for fluorescence suppression, particularly for samples (e.g., GO) where baseline fluorescence is significant. However, it is important to note that low power photobleaching is not a universal route for

reduction of fluorescence, as extended periods of photobleaching in some cases (e.g. 785 nm irradiation of GO and 532 nm irradiation of charcoal) resulted in increases in I_{base}.

S5. Fitting the Raman spectra of the reference carbons

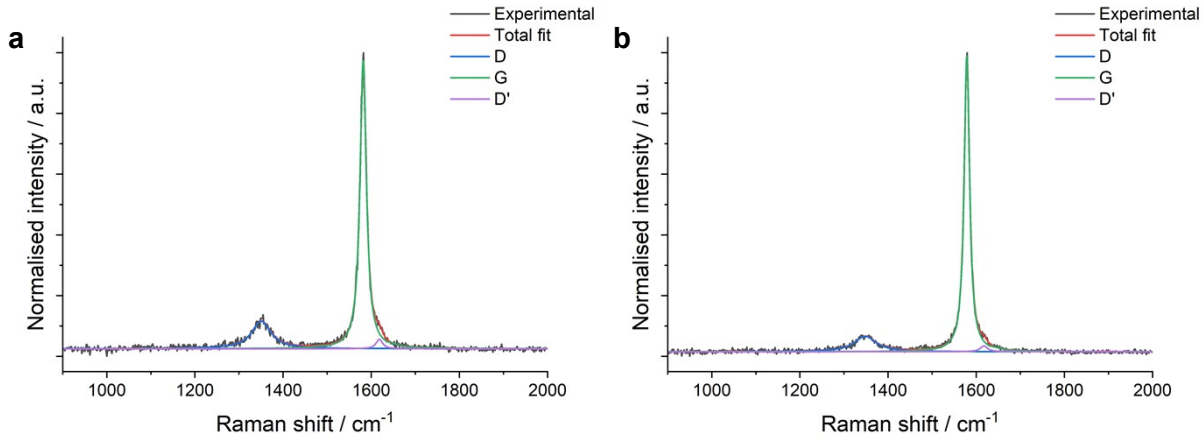

Figure S26. A representative Raman spectrum (λ = 532 nm) of graphite before (a) and after (b) thermal treatment using HyPy. The spectra have been processed as described in the Experimental section. The D and G bands could be well described using three Lorenzian lineshapes, namely the D, G and D' bands (reduced X^2 = 0.54 and 0.29 for a and b, respectively).

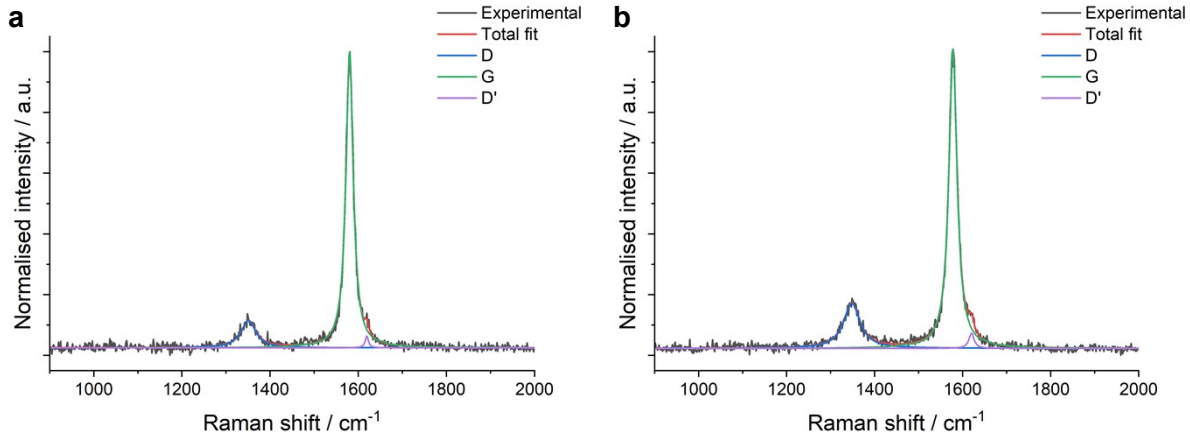

Figure S27. A representative Raman spectrum (λ = 532 nm) of MWCNT before (a) and after (b) thermal treatment using HyPy. The spectra have been processed as described in the Experimental section. The D and G bands could be well described using three Lorenzian lineshapes, namely the D, G and D' bands (reduced X^2 = 1.13 and 1.06 for a and b, respectively).

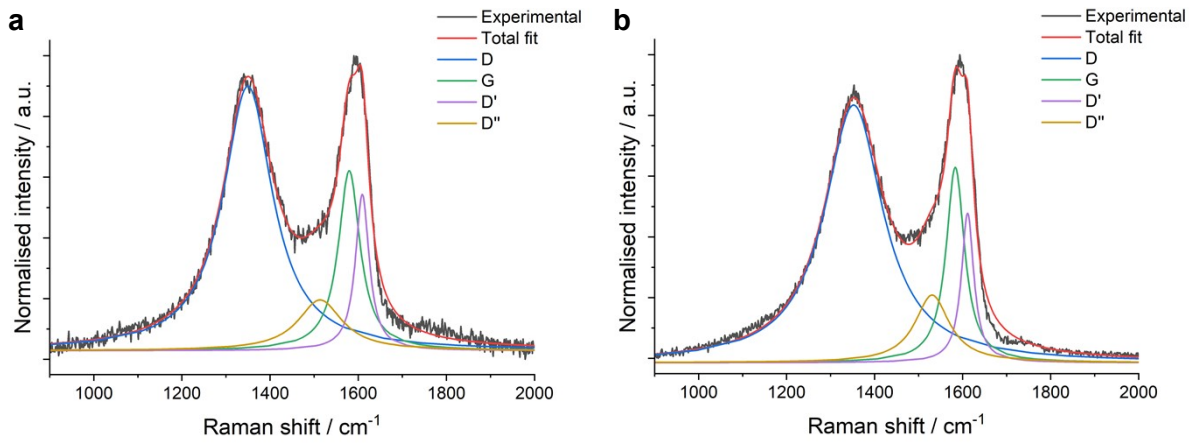

Figure S28. A representative Raman spectrum (λ = 532 nm) of GO before (a) and after (b) thermal treatment using HyPy. The spectra have been processed as described in the Experimental section. The D and G bands could be reasonably well described using four Lorenzian lineshapes, namely the D, G, D' and D'' bands (reduced X^2 = 5.20 and 4.89 for a and b, respectively). Prior to spectrum acquisition, GO not subject to thermal treatment (i.e., before) was photobleached for 100 s at p = 0.4 mW.

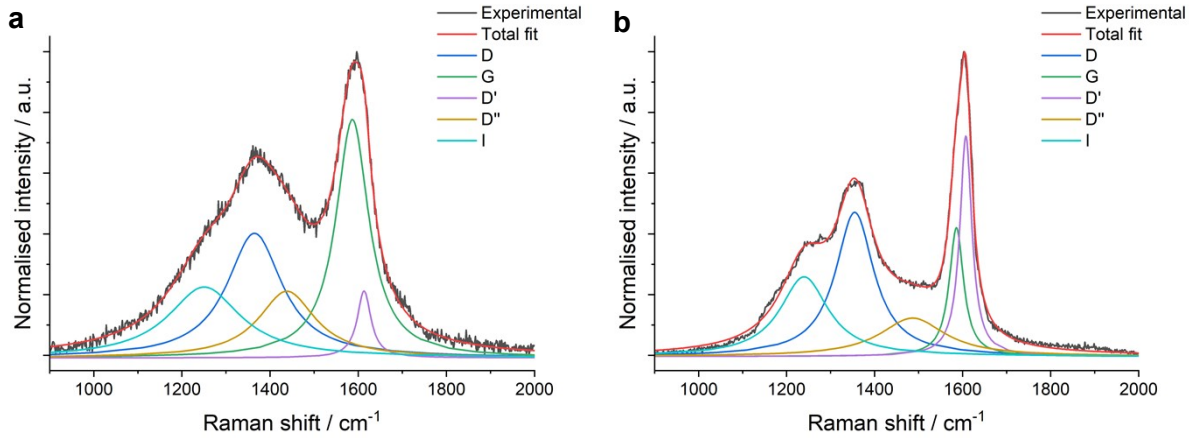

Figure S29. A representative Raman spectrum (λ = 532 nm) of charcoal before (a) and after (b) thermal treatment using HyPy. The spectra have been processed as described in the Experimental section. The D and G bands could be well described using five Lorenzian lineshapes, namely the D, G, D', D'' and I bands (reduced X^2 = 2.39 and 1.66 for a and b, respectively).

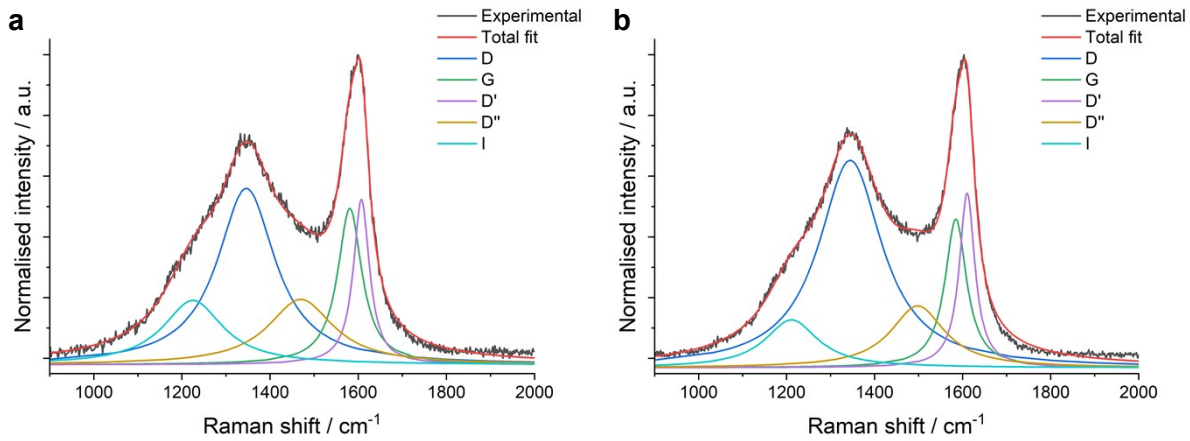

Figure S30. A representative Raman spectrum (λ = 532 nm) of Biochar-A before (a) and after (b) thermal treatment using HyPy. The spectra have been processed as described in the Experimental section. The D and G bands could be well described using five Lorenzian lineshapes, namely the D, G, D', D'' and I bands (reduced X^2 = 2.09 and 1.94 for a and b, respectively).

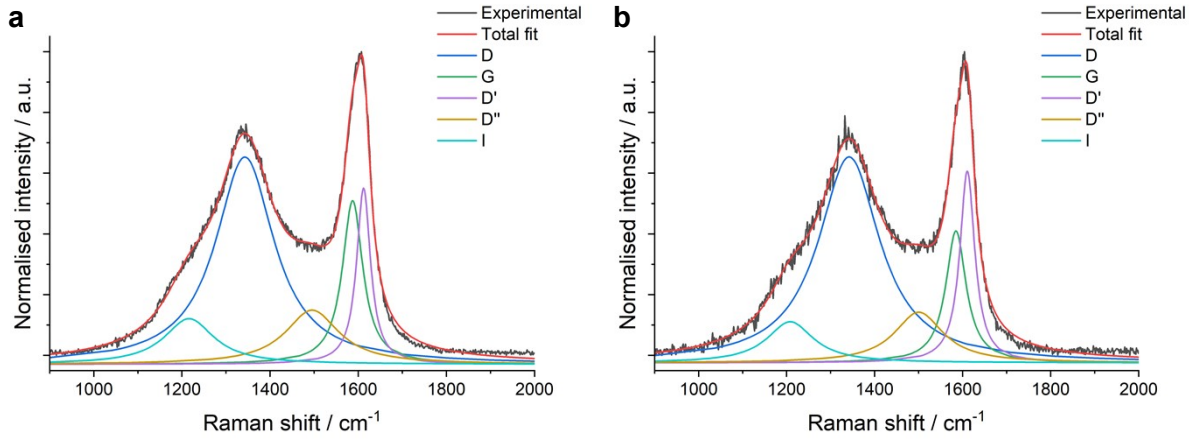

Figure S31. A representative Raman spectrum (λ = 532 nm) of Biochar-B before (a) and after (b) thermal treatment using HyPy. The spectra have been processed as described in the Experimental section. The D and G bands could be well described using five Lorenzian lineshapes, namely the D, G, D', D'' and I bands (reduced X^2 = 1.88 and 3.13 for a and b, respectively).

Table S2. Spectral characteristics extracted using the peak fitting method from the point spectra (λ = 532 nm) of the reference carbons investigated in this study by μRS before treatment and after HyPy. Values are quoted as mean plus/minus one standard deviation from N=5 measurements.

Reference carbon	Treatment	I band [a]		D band [a]		D'' band [a]		G band [a]		D' band [a]		I_D:I_G	A_D:A_G
		Position / cm^{-1}	Width / cm^{-1}	Position / cm^{-1}	Width / cm^{-1}	Position / cm^{-1}	Width / cm^{-1}	Position / cm^{-1}	Width / cm^{-1}	Position / cm^{-1}	Width / cm^{-1}		
Graphite	None	n/a	n/a	1350.4 ± 0.7	54.6 ± 2.3	n/a	n/a	1581.6 ± 0.3	19.5 ± 3.1	1620.9 ± 1.6	18.2 ± 4.0	0.14 ± 0.08	0.37 ± 0.15
	HyPy	n/a	n/a	1348.9 ± 0.8	59.4 ± 5.7	n/a	n/a	1580.0 ± 1.4	18.6 ± 4.1	1605.4 ± 13.5	45.4 ± 28.7	0.13 ± 0.09	0.39 ± 0.19
MWCNT	None	n/a	n/a	1350.9 ± 0.3	43.1 ± 3.1	n/a	n/a	1579.9 ± 0.8	21.1 ± 0.7	1620.3 ± 1.9	7.4 ± 4.9	0.11 ± 0.02	0.21 ± 0.04
	HyPy	n/a	n/a	1352.2 ± 2.3	42.6 ± 1.3	n/a	n/a	1580.2 ± 1.4	20.9 ± 1.3	1622.1 ± 0.2	8.8 ± 2.0	0.10 ± 0.03	0.21 ± 0.06
GO	None [b]	n/a	n/a	1350.0 ± 2.8	150.0 ± 15.4	1518.1 ± 7.4	119.2 ± 11.0	1578.5 ± 3.2	59.3 ± 2.8	1608.6 ± 2.3	39.3 ± 3.4	1.51 ± 0.09	3.86 ± 0.63
	HyPy	n/a	n/a	1351.5 ± 1.5	163.2 ± 3.5	1529.2 ± 1.5	95.7 ± 1.1	1579.4 ± 4.3	56.9 ± 13.9	1608.6 ± 2.4	35.5 ± 2.1	1.37 ± 0.06	4.03 ± 0.57
Charcoal	None	1248.6 ± 4.2	197.0 ± 6.6	1365.2 ± 3.3	159.7 ± 22.3	1446.0 ± 14.8	178.1 ± 20.9	1583.6 ± 3.9	95.4 ± 4.2	1610.3 ± 2.5	46.1 ± 7.6	0.68 ± 0.16	1.16 ± 0.42
	HyPy	1242.4 ± 1.6	136.1 ± 2.5	1356.7 ± 1.1	104.9 ± 3.0	1475.0 ± 8.7	195.8 ± 9.2	1584.1 ± 1.5	39.4 ± 2.2	1606.6 ± 0.7	35.7 ± 1.5	1.13 ± 0.06	3.04 ± 0.36
Biochar-A	None	1219.8 ± 6.6	156.6 ± 10.8	1344.8 ± 2.5	164.8 ± 8.2	1478.5 ± 7.4	162.2 ± 13.0	1579.6 ± 2.4	63.1 ± 2.6	1606.6 ± 1.1	45.2 ± 2.4	1.30 ± 0.24	3.50 ± 0.87
	HyPy	1215.0 ± 7.8	148.5 ± 11.4	1345.7 ± 2.8	173.7 ± 6.4	1491.4 ± 7.6	153.4 ± 9.1	1584.1 ± 0.9	60.9 ± 1.6	1610.3 ± 0.6	42.4 ± 1.7	1.26 ± 0.12	3.64 ± 0.55
Biochar-B	None	1220.7 ± 6.9	144.1 ± 5.3	1344.7 ± 3.4	155.8 ± 5.5	1484.5 ± 10.0	155.7 ± 9.0	1585.8 ± 1.3	57.2 ± 1.0	1611.0 ± 1.2	39.6 ± 1.2	1.21 ± 0.05	3.27 ± 0.53
	HyPy	1209.2 ± 4.7	130.2 ± 8.8	1341.6 ± 1.5	166.8 ± 5.7	1498.3 ± 3.4	141.8 ± 7.1	1585.2 ± 0.7	56.1 ± 0.9	1610.2 ± 0.4	40.6 ± 0.8	1.36 ± 0.07	4.32 ± 0.46

[a] Sadesky *et al.* (Carbon 43 (2005) 1731-1742) summarised the names, positions and assignments of the first-order Raman bands as follows: I band (~1200 cm^{-1}, disordered graphitic lattice mode of A_{1g} symmetry), D band (~1350 cm^{-1}, disordered graphitic lattice mode of A_{1g} symmetry), D'' band (~1500 cm^{-1}, amorphous carbon), G band (graphitic lattice mode of E_{2g} symmetry), and D' band (~1620 cm-1, disordered graphitic lattice mode of E_{2g} symmetry).

[b] Prior to spectrum acquisition, GO not subject to thermal treatment (i.e., before) was photobleached for 100 s at P = 0.4 mW.

S6. The effect of HyPy at different temperatures on the structure of Biochar-A

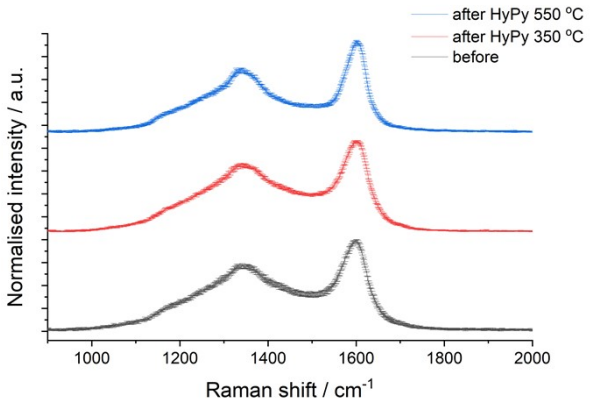

Figure S32. Mean Raman spectra (λ = 532 nm) of Biochar-A before treatment (black), after HyPy at 350 °C (red), and after HyPy at 550 °C (blue). Error bars reflect one standard deviation from N=5 measurements. The spectra have been processed as described in the Experimental section.

Table S3. Spectral characteristics extracted using the peak limits method from the point spectra (λ = 532 nm) of Biochar-A before treatment, after HyPy at 350 °C and after HyPy at 550 °C. Values are quoted as mean plus/minus one standard deviation from N=5 measurements.

Treatment	**I_{base} / counts s^{-1}**	**D band**		**G band**		**I_D:I_G**
		Position / cm^{-1}	**Width / cm^{-1}**	**Position / cm^{-1}**	**Width / cm^{-1}**	
None	33.0 ± 29.3	1338.8 ± 7.6	274.6 ± 2.7	1599.2 ± 3.5	84.8 ± 4.7	0.73 ± 0.02
HyPy (350 °C)	10.7 ± 2.2	1341.0 ± 4.0	274.0 ± 2.4	1598.3 ± 3.4	86.4 ± 2.8	0.74 ± 0.01
HyPy (550 °C)	32.8 ± 22.4	1339.1 ± 2.4	192.8 ± 13.5	1601.1 ± 1.1	63.1 ± 1.3	0.70 ± 0.02

S7. The effect of NPy on the structure of the reference carbons

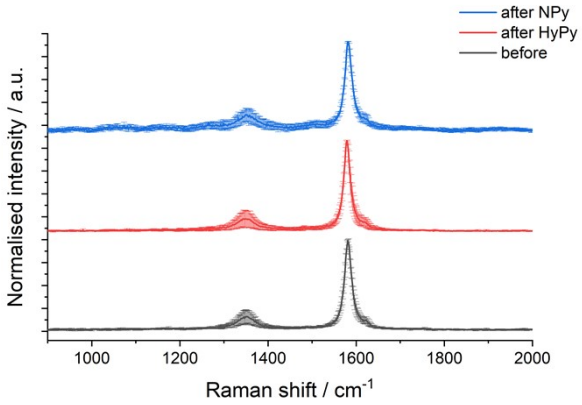

Figure S33. Mean Raman spectra (λ = 532 nm) of graphite before treatment (black), after HyPy (red) and after NPy (blue). Error bars reflect one standard deviation from N=5 measurements. The spectra have been processed as described in the Experimental section.

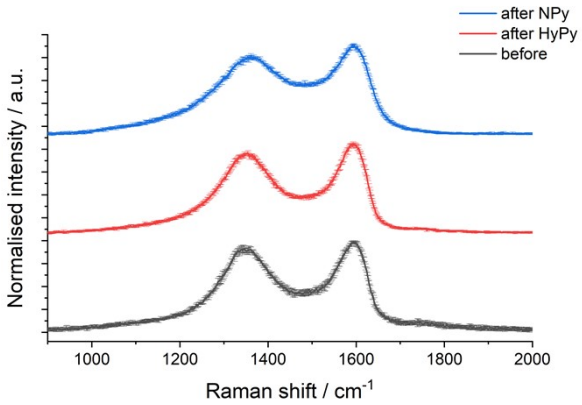

Figure S34. Mean Raman spectra (λ = 532 nm) of GO before treatment (black), after HyPy (red) and after NPy (blue). Error bars reflect one standard deviation from N=5 measurements. The spectra have been processed as described in the Experimental section. Prior to spectrum acquisition, GO not subject to thermal treatment (i.e., before) was photobleached for 100 s at P = 0.4 mW.

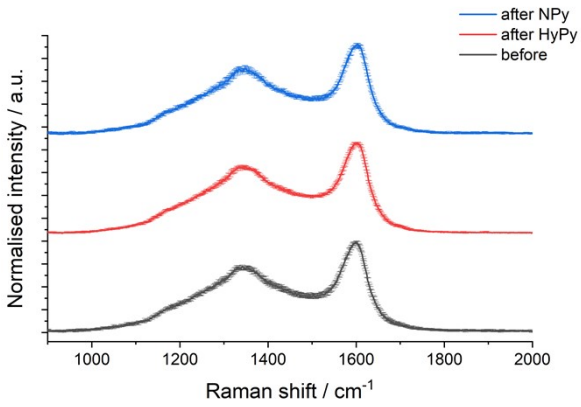

Figure S35. Mean Raman spectra (λ = 532 nm) of Biochar-A before treatment (black), after HyPy (red) and after NPy (blue). Error bars reflect one standard deviation from N=5 measurements. The spectra have been processed as described in the Experimental section.

Table S4. Spectral characteristics extracted using the peak limits method from the point spectra (λ = 532 nm) of Graphite, GO and Bichar-A before treatment, after HyPy and after NPy. Values are quoted as mean plus/minus one standard deviation from N=5 measurements.

Reference carbon	**Treatment**	**I_{base} / counts s^{-1}**	**D band**		**G band**		**I_D:I_G**
			Position / cm^{-1}	**Width / cm^{-1}**	**Position / cm^{-1}**	**Width / cm^{-1}**	
Graphite	None	1.8 ± 0.1	1351.9 ± 2.6	52.0 ± 3.7	1581.3 ± 1.3	21.4 ± 2.5	0.17 ± 0.07
	HyPy	1.3 ± 0.1	1350.3 ± 6.7	54.5 ± 3.5	1579.7 ± 0.7	19.8 ± 4.2	0.15 ± 0.09
	NPy	11.9 ± 2.6	1352.8 ± 2.9	59.9 ± 14.1	1581.3 ± 0.7	22.6 ± 1.8	0.21 ± 0.07
GO	None [a]	92.6 ± 49.3	1348.0 ± 10.0	163.0 ± 14.2	1593.1 ± 3.2	103.5 ± 6.5	0.93 ± 0.03
	HyPy	6.9 ± 1.7	1354.1 ± 5.1	158.6 ± 5.0	1593.4 ± 4.2	93.6 ± 2.1	0.90 ± 0.01
	NPy	13.8 ± 1.9	1360.8 ± 5.3	239.8 ± 3.8	1594.6 ± 1.7	140.0 ± 0.7	0.89 ± 0.02
Biochar-A	None	33.0 ± 29.3	1338.8 ± 7.6	274.6 ± 2.7	1599.2 ± 3.5	84.8 ± 4.7	0.73 ± 0.02
	HyPy	10.7 ± 2.2	1341.0 ± 4.0	274.0 ± 2.4	1598.3 ± 3.4	86.4 ± 2.8	0.74 ± 0.01
	NPy	16.1 ± 2.3	1350.9 ± 4.3	270.4 ± 1.6	1601.7 ± 1.8	82.6 ± 0.9	0.74 ± 0.02

[a] Prior to spectrum acquisition, GO not subject to thermal treatment (i.e., before) was photobleached for 100 s at P = 0.4 mW.

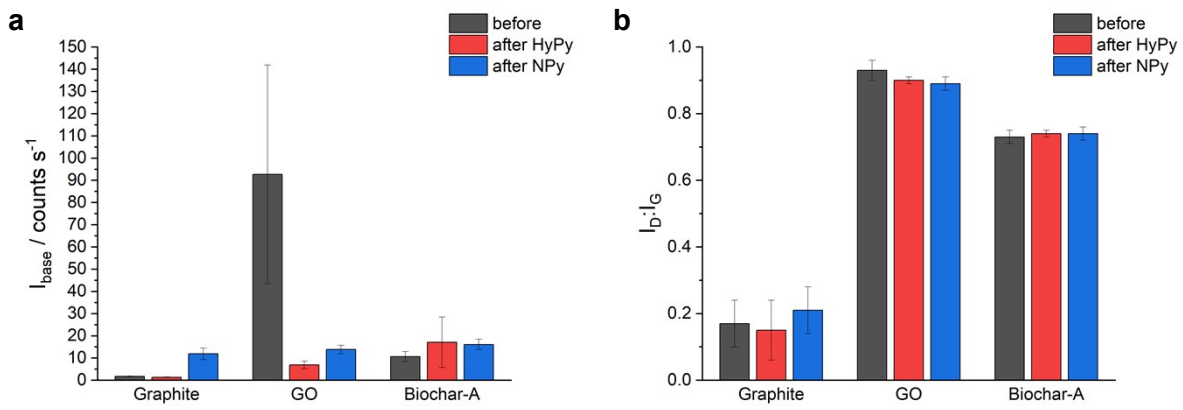

Figure S36. (a) I_{base} and (b) I_D:I_G before treatment (black), after HyPy (red) and after NPy (blue) for three of the reference carbons investigated in this study. Error bars reflect one standard deviation from N=5 measurements. Prior to spectrum acquisition, GO not subject to thermal treatment (i.e., before) was photobleached for 100 s at P = 0.4 mW.

S8. The dominance of fluorescence in the Raman spectra of the IDIDs

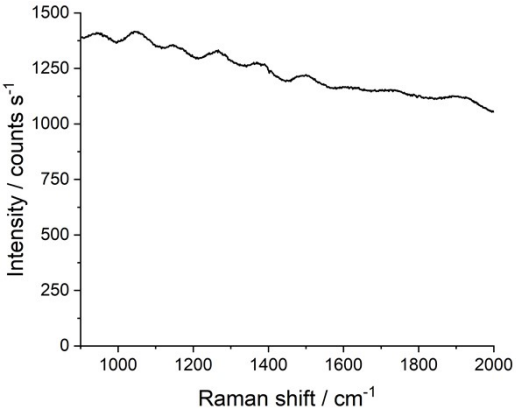

Figure 37. A representative Raman spectrum (λ = 532 nm) of IDID-A prior to treatment using HyPy. Our detector saturates above ~60000 counts (i.e., ~1000 counts s^{-1} for a 60 s acquisition) with the artefact ripples noted in the spectrum above consistent with detector saturation. As such, for IDIDs where I_{base} > 1000 counts s^{-1}, it is not possible to obtain meaningful Raman spectra as the baseline is above the detector saturation limit. It is important to note that where I_{base} = ~500-1000 counts s^{-1} it is still not possible to collect Raman spectra as some of the peak signature of the carbons (i.e., the D and G bands) will be above the saturation limit, even if the baseline adjacent to the peaks is not. Reducing the spectrum acquisition time will decrease the intensity of the baseline, but, particularly for IDIDs, long acquisition times were essential to confer sufficient signal-to-noise ratio that peak parameters could be extracted.

S9. The effect of photobleaching at low laser power on the Raman spectra of the IDIDs

Experiment:

A Raman spectrum (acquisition time = 2 s) was obtained every 2.5 s over a 300 s duration and I_{base} (the intensity at 1900 cm^{-1}) extracted at each time point. The experiments were performed separately at λ = 325 (a), 532 (b), 660 (c) and 785 nm (d).

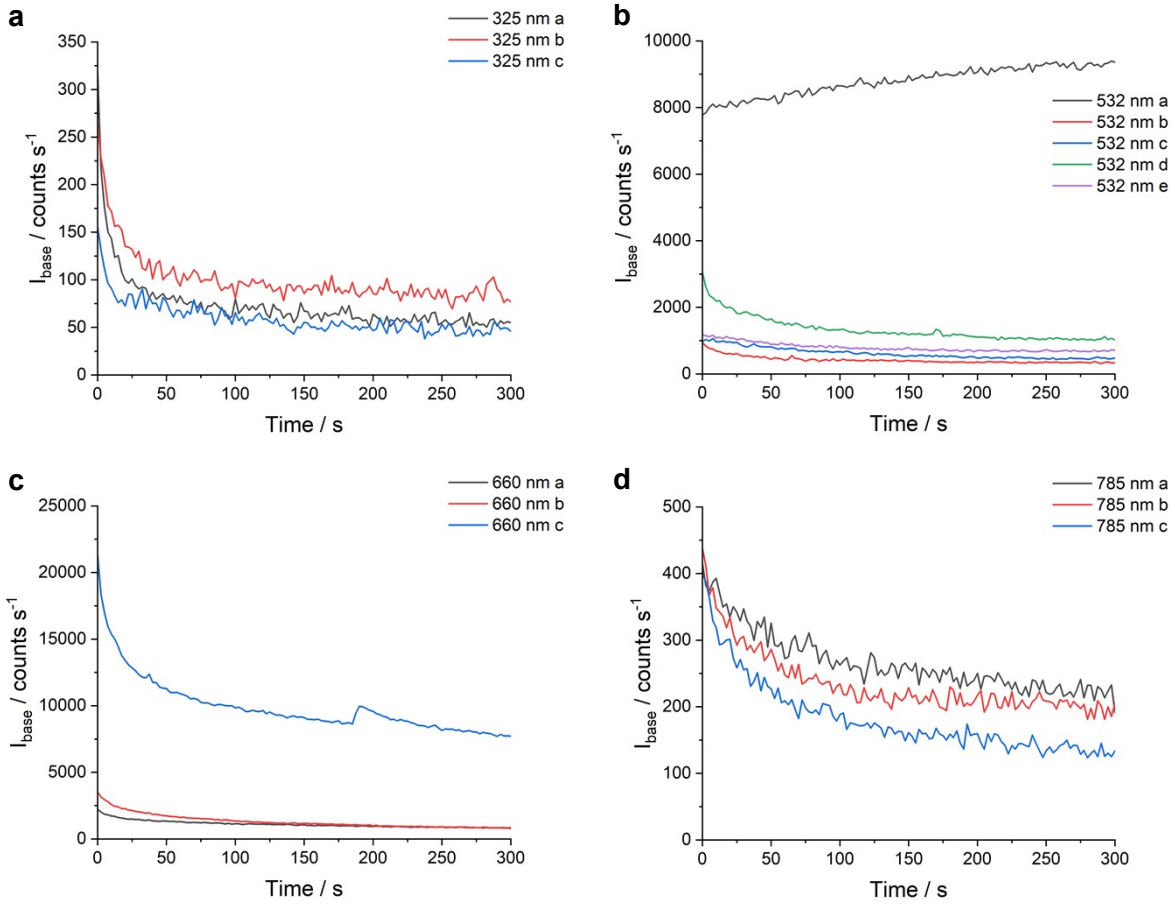

Figure S38. The effect of photobleaching IDID-A (λ = 325, 532, 660 and 785 nm) at low power over time.

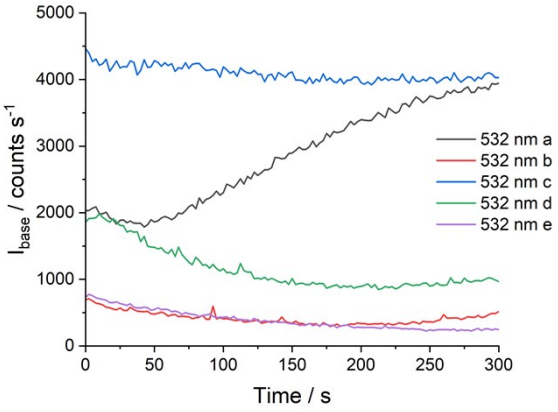

Figure S39. The effect of photobleaching IDID-B (λ = 532 nm) at low power over time.

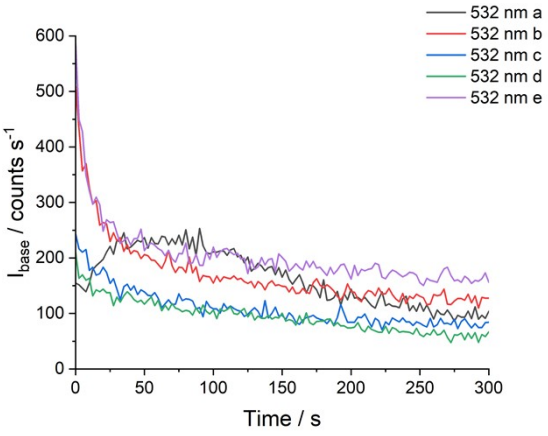

Figure S40. The effect of photobleaching IDID-C (λ = 532 nm) at low power over time.

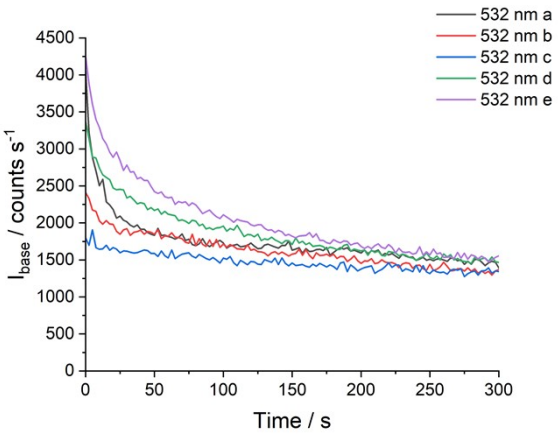

Figure S41. The effect of photobleaching IDID-D (λ = 532 nm) at low power over time.

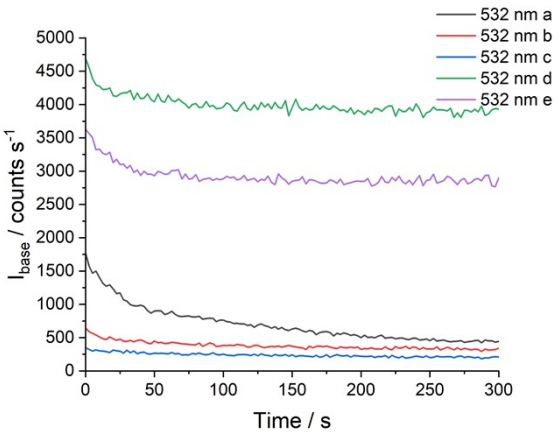

Figure S42. The effect of photobleaching IDID-E (λ = 532 nm) at low power over time.

Table S5. Mean I_{base} plus/minus one standard deviation from N=5 measurements for λ = 532 nm and N = 3 measurements for λ = 325, 660 and 785 nm for the five IDIDs analysed by μRS in this study.

IDID	**I_{base} / counts s^{-1}** [a]			
	325 nm	**532 nm**	**660 nm**	**785 nm**
IDID-A	59.3 ± 15.9	2345.6 ± 3935.7	3119.7 ± 3984.6	245.7 ± 76.9
IDID-B	- [b]	1940.9 ± 1885.5	- [b]	- [b]
IDID-C	- [b]	107.7 ± 35.3	- [b]	- [b]
IDID-D	- [b]	1424.4 ± 81.0	- [b]	- [b]
IDID-E	- [b]	1565.9 ± 1730.2	- [b]	- [b]

[a] I_{base} was extracted from the final data point within the time maps, i.e., after 300 s photobleaching at p ≤ 0.4 mW.

[b] Time maps not recorded.

Conclusions:

The multiple-wavelength, time-dependent analysis of IDID-A indicates significant fluorescence when visible (λ = 532 and 660 nm) excitation laser sources are used, some of which can be removed by low-power (P ≤ 0.4 mW) photobleaching. However, I_{base} after 5 minutes photobleaching was still too high to enable meaningful Raman spectra to be obtained. In addition, as seen during the analysis of some of the reference samples, low-power photobleaching increases I_{base} in a small number of cases.

S10. The effect of HyPy and NPy on the structure of the IDIDs

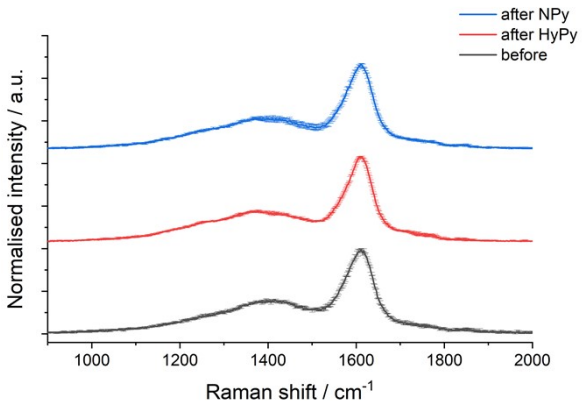

Figure S43. Mean Raman spectra (λ = 325 nm) of IDID-A before treatment (black), after HyPy (red), and after NPy (blue). Error bars reflect one standard deviation from N=3 measurements. The spectra have been processed as described in the Experimental section. Prior to spectrum acquisition, IDID-A not subject to thermal treatment (i.e., before) was photobleached for 300 s at P = 0.3 mW.

Table S6. Spectral characteristics extracted using the peak limits method from the point spectra (λ = 325 nm) of IDID-A before treatment, after HyPy and after NPy. Values are quoted as mean plus/minus one standard deviation from N=3 measurements.

Treatment	**I_{base} / counts s^{-1}**	**D band**		**G band**		**I_D:I_G**
		Position / cm^{-1}	**Width / cm^{-1}**	**Position / cm^{-1}**	**Width / cm^{-1}**	
None [a]	50.3 ± 20.8	1388.1 ± 3.1	293.3 ± 6.2	1608.3 ± 0.8	69.6 ± 1.3	0.41 ± 0.01
HyPy	29.0 ± 10.0	1369.0 ± 1.8	317.9 ± 5.2	1608.2 ± 0.3	66.1 ± 0.2	0.39 ± 0.00
NPy	29.8 ± 5.1	1375.1 ± 9.4	309.4 ± 5.3	1608.0 ± 1.2	68.8 ± 1.2	0.39 ± 0.03

[a] Prior to spectrum acquisition, IDID-A not subject to thermal treatment (i.e., before) was photobleached for 300 s at P = 0.3 mW.

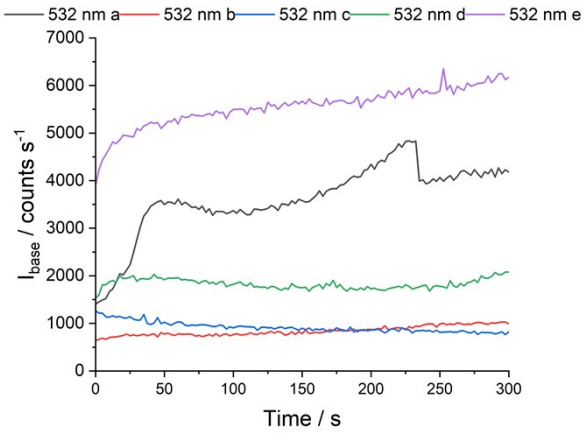

Figure S44. The effect of photobleaching IDID-A (λ = 532 nm) post-NPy treatment at low power over time. These measurements indicate that NPy and subsequent photobleaching are largely ineffective at removing the fluorescence which complicates analysis by µRS.

S11. Fitting the Raman spectra of the IDIDs

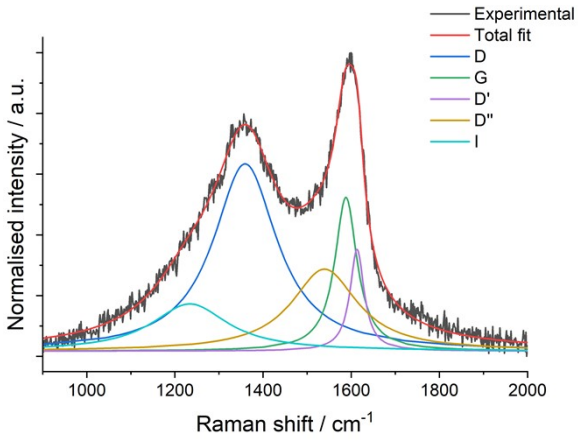

Figure S45. A representative Raman spectrum (λ = 532 nm) of IDID-A following thermal treatment using HyPy. The spectra have been processed as described in the Experimental section. The D and G bands could be reasonably well described using five Lorenzian lineshapes, namely the D, G, D', D'' and I bands (reduced X^2 = 5.40).

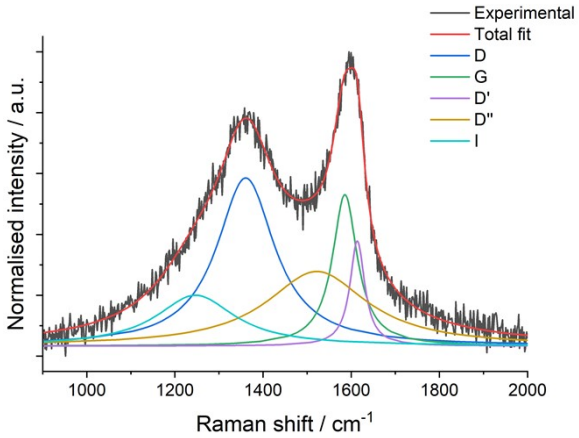

Figure S46. A representative Raman spectrum (λ = 532 nm) of IDID-B following thermal treatment using HyPy. The spectra have been processed as described in the Experimental section. The D and G bands could be reasonably well described using five Lorenzian lineshapes, namely the D, G, D', D'' and I bands (reduced X^2 = 9.35).

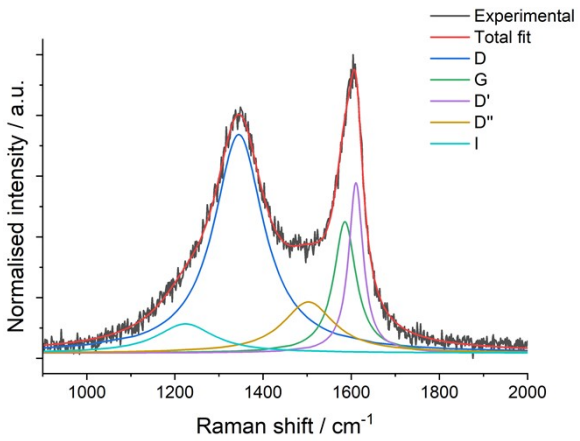

Figure S47. A representative Raman spectrum (λ = 532 nm) of IDID-C following thermal treatment using HyPy. The spectra have been processed as described in the Experimental section. The D and G bands could be reasonably well described using five Lorenzian lineshapes, namely the D, G, D', D'' and I bands (reduced X^2 = 4.17).

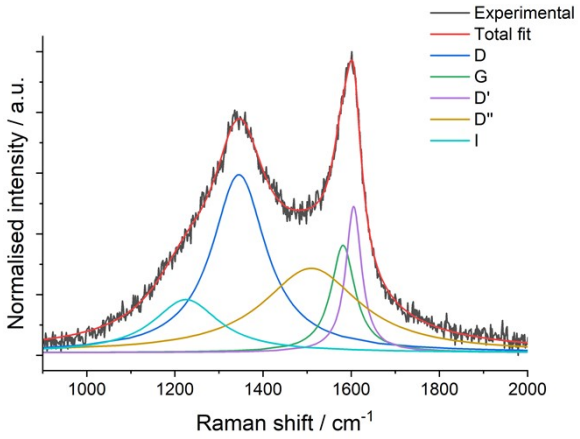

Figure S48. A representative Raman spectrum (λ = 532 nm) of IDID-D following thermal treatment using HyPy. The spectra have been processed as described in the Experimental section. The D and G bands could be reasonably well described using five Lorenzian lineshapes, namely the D, G, D', D'' and I bands (reduced X^2 = 4.06).

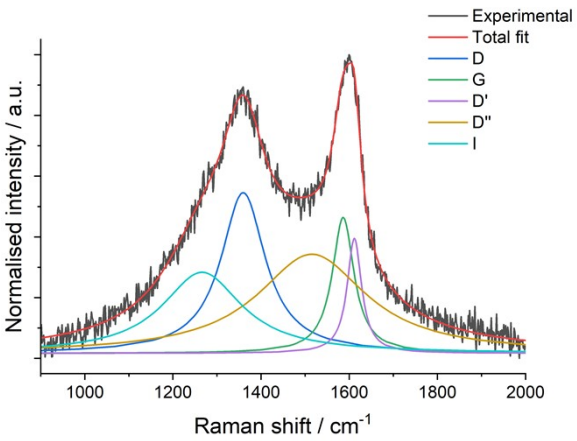

Figure S49. A representative Raman spectrum (λ = 532 nm) of IDID-E following thermal treatment using HyPy. The spectra have been processed as described in the Experimental section. The D and G bands could be reasonably well described using five Lorenzian lineshapes, namely the D, G, D', D'' and I bands (reduced X^2 = 8.02).

Table S7. Spectral characteristics extracted using the peak fitting method from the point spectra (λ = 532 nm) of the IDIDs after HyPy treatment investigated in this study by µRS. Values are quoted as mean plus/minus one standard deviation from N=5 measurements.

IDID	**I band**		**D band**		**D'' band**		**G band**		**D' band**		**I_D:I_G**	**A_D:A_G**
	Position / cm^{-1}	**Width / cm^{-1}**	**Position / cm^{-1}**	**Width / cm^{-1}**	**Position / cm^{-1}**	**Width / cm^{-1}**	**Position / cm^{-1}**	**Width / cm^{-1}**	**Position / cm^{-1}**	**Width / cm^{-1}**		
IDID-A	1232.2 ± 21.9	187.8 ± 20.7	1363.2 ± 5.7	194.1 ± 27.9	1543.7 ± 14.4	162.6 ± 46.7	1583.4 ± 3.7	61.4 ± 1.4	1610.3 ± 2.3	43.2 ± 4.6	1.40 ± 0.19	4.50 ± 1.27
IDID-B	1215.8 ± 34.8	215.3 ± 40.1	1357.1 ± 7.1	181.8 ± 30.4	1535.0 ± 19.8	240.5 ± 74.5	1583.1 ± 8.3	69.5 ± 11.2	1611.1 ± 5.1	43.8 ± 5.8	1.45 ± 0.19	3.94 ± 1.40
IDID-C	1194.9 ± 19.4	186.6 ± 19.0	1344.5 ± 1.2	154.5 ± 15.7	1507.8 ± 5.9	136.9 ± 21.5	1580.1 ± 7.0	64.2 ± 4.3	1607.0 ± 3.9	45.7 ± 6.7	1.98 ± 0.58	4.78 ± 1.49
IDID-D	1231.5 ± 8.4	196.2 ± 16.9	1347.5 ± 2.3	149.3 ± 7.5	1505.6 ± 8.0	136.9 ± 21.5	1578.4 ± 5.2	70.5 ± 7.1	1605.5 ± 1.7	70.5 ± 7.1	1.71 ± 0.18	3.64 ± 0.45
IDID-E	1253.3 ± 21.0	192.8 ± 33.8	1357.5 ± 2.6	144.5 ± 22.2	1521.4 ± 18.7	271.4 ± 39.7	1584.4 ± 3.3	60.5 ± 3.1	1610.8 ± 2.2	41.6 ± 5.1	1.45 ± 0.39	3.57 ± 1.58

S12. Other IDIDs studied

Table S8. Technical details of the IDIDs analysed by GC-MS in this study, including the location engine component failed, the fuel used and the quoted complaint. CARB = Californian Air Resources Board. ULSD = Ultra-low sulphur diesel. PIBSI = Polyisobutylene succinimide.

IDID	Location	Fuel	Complaint
IDID-F	California	CARB diesel	The complaint was the engine not starting.
IDID-G	Illinois	ULSD	The complaint was insufficient power, later identified by the injector being stuck.
IDID-H	DW10B engine test	RF06 with low molecular weight PIBSI	After 16 hours testing, there was a severe failure due to the injector being jammed.
IDID-I	Mid-west USA	ULSD	The complaint was drivability issues, later identified by the injector being stuck.
IDID-J	Norway	EN590	The complaint was failure to start due to a stuck injector.